https://doi.org/10.5194/egusphere-2026-4234
Preprint. Discussion started: 6 August 2026

Arctic Polar Vortex Strengthening on Seasonal Scales After Extreme Solar Proton Events: Quantitative Evidence for an Ozone–Dynamics Feedback

Yaxuan Li[1,2], Hui Li[1,2], Yuting Wang[1,2], Yilin Liu[1,2], Yudi Pan[3], Wei Xu[3], and Chi Wang[1,2]

[1]State Key Laboratory of Solar Activity and Space Weather, National Space Science Center, Chinese Academy of Sciences, Beijing, 100190, China
[2]University of Chinese Academy of Sciences, Beijing, China
[3]Department of Space Physics, School of Earth and Space Science and Technology, Wuhan University, Wuhan, China

Correspondence: Hui Li (hli@nssc.ac.cn)

Abstract. Energetic particle precipitation (EPP) has long been known to influence the polar middle atmosphere. Extreme solar proton events (SPEs), the most intense type of EPP, are expected to influence the Arctic polar vortex (APV); however, their impacts and underlying pathways remain poorly understood. Here, we examine APV variability and the associated stratospheric processes following the two most extreme late-October SPEs, using the ERA5 reanalysis data. Both events were followed by persistent ozone depletion, cooling of the polar stratosphere, and sustained strengthening of the APV from autumn into late winter and spring. The ozone, temperature, and APV anomalies evolve coherently over time, with the APV transitioning from a relatively weak background state to a strongly enhanced state with respect to the climatological distribution. Thermodynamic budget diagnostics reveal that the temperature anomalies were dominated by dynamical cooling rather than by direct radiative cooling from ozone depletion. This dynamical cooling was accompanied by a tendency for downward planetary wave refraction at high latitudes and associated changes in wave–mean flow interactions. Collectively, these results provide quantitative evidence that extreme SPEs can influence the seasonal APV variability through coupled ozone and dynamical processes.

1 Introduction

Energetic particle precipitation (EPP) is a major external forcing of the polar middle atmosphere, driven by precipitating protons, electrons, and ions (Jia et al., 2024). These particles enter the polar cap regions, with higher-energy protons penetrating deeper into the atmosphere. For example, protons with energies of ∼10 MeV deposit energy near 70 km, while those with energies of ∼100 MeV can penetrate to approximately 30 km (Turunen et al., 2009). The resulting ionization produces odd hydrogen (HO_x) and odd nitrogen (NO_y), which catalyze ozone destruction (Jackman et al., 2008; Funke et al., 2011). HO_x-induced ozone depletion is typically limited to several days in the mesosphere and upper stratosphere due to the short lifetime of HO_x, whereas long-lived NO_y can descend into the stratosphere, prolonging the ozone loss for months beyond the initial forcing (Smith-Johnsen et al., 2017; Denton et al., 2018; Szeląg et al., 2022).

EPP is commonly classified into energetic electron precipitation (EEP) and solar proton events (SPEs) (Seppälä et al., 2014). EEP primarily affects the mesosphere through electrons with energies from tens of keV to several MeV (Rozanov et al.,

https://doi.org/10.5194/egusphere-2026-4234
Preprint. Discussion started: 6 August 2026

2012; Wang et al., 2024). In contrast, SPEs involve protons with energies up to hundreds of MeV and can reach the upper stratosphere (Rozanov et al., 2012; Jia et al., 2020). Observations indicate ozone reductions exceeding 50% during extreme SPEs in the polar mesosphere, compared with 10–30% during typical SPEs and less than 7% during EEP (Wang et al., 2024; Jackman et al., 2008). During extreme SPEs, high-energy protons produce in situ ionization in the upper stratosphere while strong mesospheric ozone depletion propagates downward, sustaining stratospheric anomalies for 1–2 months (Jackman et al., 2008; Jia et al., 2020).

Ozone perturbations alter the radiative heating and thereby modify the thermal structure, which can consequently influence stratospheric circulation (Silverman et al., 2018; Tian et al., 2023; Hong et al., 2025). The Arctic polar vortex (APV), a large-scale cyclonic circulation encircling the polar stratosphere, is maintained by the meridional temperature gradient between the warm tropics and the cold polar region (Schoeberl and Newman, 2015; Waugh et al., 2017). As a key feature of Arctic stratospheric dynamics, the APV is highly sensitive to temperature perturbations and can respond rapidly to radiatively induced changes in the polar stratosphere through thermal wind balance (Ward et al., 2021; Tian et al., 2023). Planetary wave (PW) forcing further modulates APV variability via wave–mean flow interactions (Oehrlein et al., 2020; Hannachi et al., 2025).

Given the sensitivity of the APV to thermal and dynamical forcings, it is plausible that EPP-induced perturbations could modulate the vortex on various timescales (Seppälä et al., 2013, 2025). For SPEs, research has primarily focused on short-term responses, with a transient strengthening of the polar vortex associated with enhanced proton flux during events (Veretenenko, 2021; Li et al., 2025). In contrast, EEP has been linked to more persistent APV variability on monthly timescales (Arsenovic et al., 2016; Salminen et al., 2019, 2020a, 2022, 2024). These longer-lasting responses have been interpreted in terms of a chemically driven pathway, whereby long-lived NO_y descends into the stratosphere and prolongs ozone depletion (Nesse et al., 2026). This mechanism has recently been proposed to trigger a positive ozone–dynamics feedback involving thermal wind adjustment and wave–mean flow interactions (Nesse et al., 2026). Whether such a feedback also operates following extreme SPEs, and whether the resulting APV anomalies can persist on seasonal timescales through radiative and dynamical processes, remain poorly constrained observationally.

Here, we investigate the response of the APV to the two most extreme late-October SPEs, selected for their exceptionally high proton fluences and similar stratospheric background conditions. Using ERA5 reanalysis together with radiative transfer calculations from the Rapid Radiative Transfer Model for GCMs (RRTMG) and transformed Eulerian-mean (TEM) diagnostics, we examine the evolution of ozone, temperature, circulation, and PW activity following the events. We focus on the persistence of the stratospheric response and the extent to which radiative and dynamical processes contribute to seasonal APV variability following extreme SPEs.

2 Dataset and Methodology

2.1 Extreme SPEs

Solar proton fluxes were obtained from energetic proton detectors onboard the Geostationary Operational Environmental Satellites (GOES), provided by the Space Weather Prediction Center (SWPC) of the National Oceanic and Atmospheric Administra-

https://doi.org/10.5194/egusphere-2026-4234
Preprint. Discussion started: 6 August 2026

tion (NOAA) as 5-minute averages. All SPEs between 1986 and March 2020 were identified using a daily mean flux threshold of 10 pfu (protons $\mathrm{cm^{-2}\,sr^{-1}\,s^{-1}}$) at energies > 10 MeV, yielding a total of 112 events. Events were ranked according to their integrated proton fluences above 10 MeV (protons cm^{-2} sr^{-1}), and the two most extreme cases, beginning on 19 October 1989 and 26 October 2003, were selected for detailed analysis. In our study, both events are characterized by exceptionally intense proton fluences and are classified as extreme SPEs, with the largest total fluences on the order of 10^9 protons cm^{-2} sr^{-1} during 1986–2020. The stratospheric background state preceding both events was dynamically stable and characterized by the easterly phase of the quasi-biennial oscillation (QBO), providing a relatively stable and consistent baseline.

2.2 Stratospheric atmospheric properties

2.2.1 ERA5 reanalysis

Stratospheric atmospheric fields were derived from the ERA5 reanalysis (Hersbach et al., 2023), the fifth-generation atmospheric reanalysis produced by the European Centre for Medium-Range Weather Forecasts (ECMWF) under the Copernicus Climate Change Service initiative (Hersbach et al., 2020). Daily ERA5 data from 1986–2020 were analyzed on pressure levels from 1 to 100 hPa over the Northern Hemisphere at a horizontal resolution of $1^\circ \times 1^\circ$. The analyzed variables include geopotential height, zonal and meridional wind, vertical velocity, temperature, and ozone mass mixing ratio.

2.2.2 APV and anomaly definition

The strength of the APV is quantified by the cosine-weighted, zonal-mean zonal wind averaged over 60°–90°N (U_{6090}) (Butler et al., 2015; Li et al., 2025). Polar-cap means (60°–90°N) of temperature, ozone, winds, and radiative and dynamical heating rates were calculated using the same cosine weighting. These quantities were used to construct pressure–time cross sections.

To remove both the seasonal cycle and pre-event background variability, anomalies are defined as

$$X_a = X_o - X_c - X_b, \tag{1}$$

where X_o denotes the original field (e.g., zonal wind, temperature, ozone, and radiative and dynamical heating rates), X_c is the climatological mean over 1986–2020, and X_b is the mean anomaly relative to the climatological mean over the 5 days preceding each event.

Response episodes are identified as consecutive periods with westerly 5-day smoothed zonal-mean zonal wind ($U_{6090} > 0$) and positive anomalies ($U_a > 0$) at 10 hPa, indicating APV strengthening. The response magnitude is quantified by ranking the mean U_{6090} during each episode against the climatological distribution for the corresponding calendar days (1986–2020), and expressing its relative position as a rank-based percentage, where Top $= \mathrm{rank}/N$ and Bottom $= (N - \mathrm{rank} + 1)/N$.

The stratospheric final warming (SFW) is defined as the final springtime reversal of the zonal-mean zonal wind from westerly to easterly at 60°N and 10 hPa (Hauchecorne et al., 2022). The corresponding day of year (DOY) is ranked within the climatological distribution to assess potential delays in vortex breakdown.

https://doi.org/10.5194/egusphere-2026-4234
Preprint. Discussion started: 6 August 2026

2.2.3 Statistical significance

Statistical significance is assessed using a Monte Carlo approach with 10,000 pseudo-events. For each of the two SPEs, onset dates are randomly selected within ±7 days of the actual onset date, and event durations are set equal to those of the observed cases. The resulting distributions of anomaly fields are used to estimate the 90% confidence intervals.

2.3 Radiative transfer calculations

Shortwave and longwave radiative heating rates were calculated using the RRTMG model (Mlawer et al., 1997; Iacono et al., 2008). The radiative impact of SPE-induced ozone changes was isolated using the partial radiative perturbation (PRP) method (Wetherald and Manabe, 1988; Klocke et al., 2013; Rieger et al., 2017). Two experiments were performed: (i) a control experiment using SPE-period temperature and climatological ozone, and (ii) a perturbed experiment using both temperature and ozone from the SPE period.

The radiative effect of ozone changes was estimated separately for shortwave (Q_{sw}) and longwave heating rates (Q_{lw}) as

$$\Delta Q = Q(\mathrm{O}_{3,\mathrm{SPE}}, T_{\mathrm{SPE}}) - Q(\mathrm{O}_{3,\mathrm{clim}}, T_{\mathrm{SPE}}), \tag{2}$$

where $Q(\mathrm{O}_3, T)$ denotes the radiative heating rate as a function of ozone and temperature. Subscripts SPE and clim refer to fields during the SPE period and their climatological counterparts. To remove any systematic bias unrelated to the SPE, the mean ΔQ during the 5-day pre-event period is subtracted from the entire time series. The total radiative heating rate is given by $Q_{\mathrm{rad}} = Q_{\mathrm{sw}} + Q_{\mathrm{lw}}$.

To quantify cooling contributions, radiative and dynamical cooling rates are defined as

$$Q^c_{\mathrm{rad}} = \begin{cases} |Q_{\mathrm{rad}}|, & Q_{\mathrm{rad}} < 0, \\ 0, & Q_{\mathrm{rad}} \geq 0, \end{cases} \tag{3}$$

$$Q^c_{\mathrm{dyn}} = \begin{cases} |Q_{\mathrm{dyn}}|, & Q_{\mathrm{dyn}} < 0, \\ 0, & Q_{\mathrm{dyn}} \geq 0. \end{cases} \tag{4}$$

The relative importance of radiative and dynamical cooling is then quantified as

$$\mathcal{R} = \frac{Q^c_{\mathrm{rad}} - Q^c_{\mathrm{dyn}}}{Q^c_{\mathrm{rad}} + Q^c_{\mathrm{dyn}}}. \tag{5}$$

Values of $\mathcal{R}$ approaching 1 indicate radiative cooling dominance, whereas values approaching -1 indicate dynamical cooling dominance.

2.4 Wave activity diagnosis

2.4.1 TEM diagnostics

PW activity is diagnosed within the TEM framework, which quantifies wave–mean flow interactions and the associated dynamical forcing (Andrews et al., 1987; Butchart, 2022). In spherical coordinates, the zonal-mean wave forcing is defined as

https://doi.org/10.5194/egusphere-2026-4234
Preprint. Discussion started: 6 August 2026

$$F_\mathrm{w} = (\rho_0 a \cos\phi)^{-1} \nabla \cdot \mathbf{F}, \tag{6}$$

where ρ_0 is the background density, a is Earth's radius, ϕ is latitude, and $\mathbf{F}$ is the Eliassen-Palm (EP) flux.

The EP flux, representing wave activity and momentum transport, is given by

$$\mathbf{F} = (0, F^{(\phi)}, F^{(z)}), \tag{7}$$

with meridional and vertical components

$$F^{(\phi)} = \rho_0 a \cos\phi \left(\bar{u}_z \frac{\overline{v'\theta'}}{\bar{\theta}_z} - \overline{u'v'} \right), \tag{8}$$

$$F^{(z)} = \rho_0 a \cos\phi \left\{ \left[f - (a\cos\phi)^{-1} \frac{\partial(\bar{u}\cos\phi)}{\partial\phi} \right] \frac{\overline{v'\theta'}}{\bar{\theta}_z} - \overline{u'w'} \right\}, \tag{9}$$

and its divergence is

$$\nabla \cdot \mathbf{F} = (a\cos\phi)^{-1} \frac{\partial}{\partial\phi}(F^{(\phi)}\cos\phi) + \frac{\partial F^{(z)}}{\partial z}. \tag{10}$$

Here, $\bar{u}$, $\bar{v}$, and $\bar{w}$ denote the zonal-mean zonal wind, meridional wind, and vertical velocity, respectively; $\overline{u'v'}$, $\overline{u'w'}$, and $\overline{v'\theta'}$ are eddy fluxes of momentum and heat; $\bar{\theta}_z$ is the vertical gradient of potential temperature; and f is the Coriolis parameter.

The residual mean meridional and vertical circulations are defined as

$$\bar{v}^* = \bar{v} - \rho_0^{-1} \frac{\partial}{\partial z} \left(\rho_0 \frac{\overline{v'\theta'}}{\bar{\theta}_z} \right), \tag{11}$$

$$\bar{w}^* = \bar{w} + (a\cos\phi)^{-1} \frac{\partial}{\partial\phi} \left(\cos\phi \frac{\overline{v'\theta'}}{\bar{\theta}_z} \right). \tag{12}$$

2.4.2 Dynamical heating

The associated dynamical heating is calculated as

$$Q_\mathrm{dyn} = -\frac{\bar{T}}{\bar{\theta}} \left(a^{-1} \bar{v}^* \frac{\partial\bar{\theta}}{\partial\phi} + \bar{w}^* \frac{\partial\bar{\theta}}{\partial z} \right), \tag{13}$$

where $\bar{T}$ and $\bar{\theta}$ are the zonal-mean temperature and potential temperature. Q_dyn is expressed in units consistent with the radiative heating rates.

The net heating rate is given by $Q_\mathrm{net} = Q_\mathrm{rad} + Q_\mathrm{dyn}$.

2.4.3 PW propagation

PW propagation is further characterized using the refractive index (Li et al., 2007),

$$n_k^2(y,z) = \frac{\bar{q}_\phi}{\bar{u}} - \left(\frac{k}{a\cos\phi} \right)^2 - \left(\frac{f}{2NH} \right)^2, \tag{14}$$

where

$$\bar{q}_\phi = \frac{2\Omega}{a}\cos\phi - \frac{1}{a^2}\left[\frac{(\bar{u}\cos\phi)_\phi}{\cos\phi}\right]_\phi - \frac{f^2}{\rho_0}\left(\rho_0\frac{\bar{u}_z}{N^2}\right)_z, \tag{15}$$

and Ω, N, H, and k denote Earth's rotation rate, buoyancy frequency, scale height, and zonal wavenumber, respectively. Positive n_k^2 indicates regions where PWs can propagate, with larger values favouring wave propagation, whereas waves tend to refract away from regions with negative n_k^2 (Matsuno, 1970; Li et al., 2007).

PW amplitudes are diagnosed at 10 hPa and 60°N from geopotential height (Shi et al., 2021; Liu et al., 2022). Zonal anomalies relative to the daily climatology are first computed and then decomposed into zonal wavenumbers using Fourier analysis. The amplitudes of individual wavenumbers ($k = 1,2$) are defined as the magnitude of the corresponding Fourier coefficients (Shi et al., 2021).

3 Results

3.1 The seasonal strengthening of the Arctic APV after extreme SPEs

Fig. 1a,b presents the evolution of solar proton flux. Both daily fluxes exceed 10 pfu at energies $> 100\,\mathrm{MeV}$, indicating penetration into the stratosphere, while fluxes at energies $> 10\,\mathrm{MeV}$ reach $\sim 10^3$ pfu, sufficient to produce substantial ionization in the middle atmosphere and to sustain a downward-propagating chemical perturbation into the stratosphere.

Fig. 1c–h presents the evolution of polar ozone (Fig. 1c,d), temperature (Fig. 1e,f), and zonal wind anomalies (Fig. 1g,h) averaged over 60°–90°N from the SPE onset to the subsequent springtime vortex breakdown for the 1989 (SPE1) and 2003 (SPE2) events. Based on the criteria defined above, four APV response episodes (E1–E4) are identified.

Following the SPE onset, the ozone depletion exhibits a downward migration from the upper stratosphere in autumn to the middle and lower stratosphere in spring. During late autumn and early winter (E1 and E3), pronounced ozone depletion emerges primarily in the upper stratosphere (Fig. 1c,d), reaching -0.8 and -0.9 ppmm, corresponding to 9.7% and 10.5% decreases relative to the 5-day pre-event mean in the 1–10 hPa layer. This is accompanied by pronounced cooling (Fig. 1e,f) and a strengthened polar vortex (Fig. 1g,h), with positive mean U_{6090} anomalies reaching 9.7 and 17.7 m s^{-1} in the upper stratosphere. By mid-December in E1, the ozone depletion extends downward into the middle stratosphere. There, enhanced depletion (enclosed by the -0.6 and -0.9 ppmm contours) coincides with stronger cooling (enclosed by the -4 and -8 K contours) and a concurrent strengthening of the westerlies. In E3, pronounced ozone depletion develops simultaneously in the upper and middle stratosphere following the SPE onset. Distinct anomaly centers of ozone depletion, cooling, and strengthened westerlies occur at similar times in the middle stratosphere, indicating a coherent temporal evolution of the three fields.

The wintertime evolution is interrupted by sudden stratospheric warmings (SSW), including a minor SSW following E1 and a major SSW following E3. These events temporarily reverse the westerly circulation into easterlies and induce transient warming (Fig. 1e–f) and enhanced PW activity (Fig. 1i–j). At the same time, the associated strong vertical transport facilitates the downward propagation of SPE-induced perturbations from the mesosphere into the stratosphere, shifting the ozone depletion signal toward the middle and lower stratosphere (Baldwin et al., 2021).

https://doi.org/10.5194/egusphere-2026-4234
Preprint. Discussion started: 6 August 2026

In spring (E2 and E4), ozone depletion becomes more pronounced in the 10–100 hPa layer, reaching −0.5 and −0.7 ppmm (9.7% and 13.0%), while the upper-stratospheric depletion both weaken to approximately −0.3 ppmm (3.3% and 3.5%). During E2, three distinct maxima in ozone depletion develop in the middle stratosphere and coincide with vertically coherent cooling anomalies, while the westerly anomalies strengthen simultaneously. In E4, pronounced ozone depletion persists throughout the middle stratosphere, while the strongest cooling and westerly anomalies progressively evolve downward during the recovery from the major SSW.

Overall, APV strengthening persisted for 202 and 186 days following the two extreme SPEs, corresponding to approximately 6–7 months from late autumn to the following spring. Throughout the identified response episodes, the vortex evolved from a relatively weak background state to a strongly enhanced state, in line with its rank-based position within the climatological distribution shown in Table 1. Springtime peaks reached the top 8.6% and 14.3% of the climatological distribution for E2 and E4, respectively. The corresponding final warming dates ranked within the top 11.4% and 28.6% of the climatological distribution (Table 1), indicating a tendency toward delayed vortex breakdown.

Table 1. Key characteristics and stratospheric dynamical responses associated with two extreme SPEs.

	SPE1 (1989/10/19)		SPE2 (2003/10/26)	
Proton fluence (protons cm^{-2} sr^{-1})	1.54×10^9		1.27×10^9	
Episode	E1	E2	E3	E4
Start date	1989/10/19	1990/02/16	2003/10/26	2004/02/17
End date	1990/02/08	1990/05/08	2003/12/20	2004/04/28
APV anomaly (m s^{-1})	6.0	12.2	13.5	19.6
Background APV rank	27/35 (Bottom 25.7%)	–	30/35 (Bottom 17.1%)	–
APV rank	8/34 (Top 23.5%)	3/35 (Top 8.6%)	8/35 (Top 22.9%)	5/35 (Top 14.3%)
Final warming date (DOY)	128		120	
Final warming rank	4/35 (Top 11.4%)		10/35 (Top 28.6%)	

Ranks are calculated relative to the climatological distribution during 1986–2020, with rank 1 indicating the strongest APV anomaly or the latest final warming date. Relative positions are expressed as Top or Bottom percentages as defined in Section 2.2.2. The background APV rank is defined as the mean APV over the 5 days preceding each SPE event. For E1, $N = 34$ because the analysis period spans two calendar years, leaving no complete sample for the final year (2020); otherwise, $N = 35$.

3.2 Radiative and dynamical contributions to polar cooling

The strengthened APV is accompanied by persistent polar cooling (Fig. 1). Through thermal wind balance, such cooling would be expected to support enhanced stratospheric westerlies and thus contribute to vortex strengthening. To determine the processes that maintain this cooling, we examine the relative contributions of radiative and dynamical heating anomalies following the SPEs (Fig. 2).

https://doi.org/10.5194/egusphere-2026-4234
Preprint. Discussion started: 6 August 2026

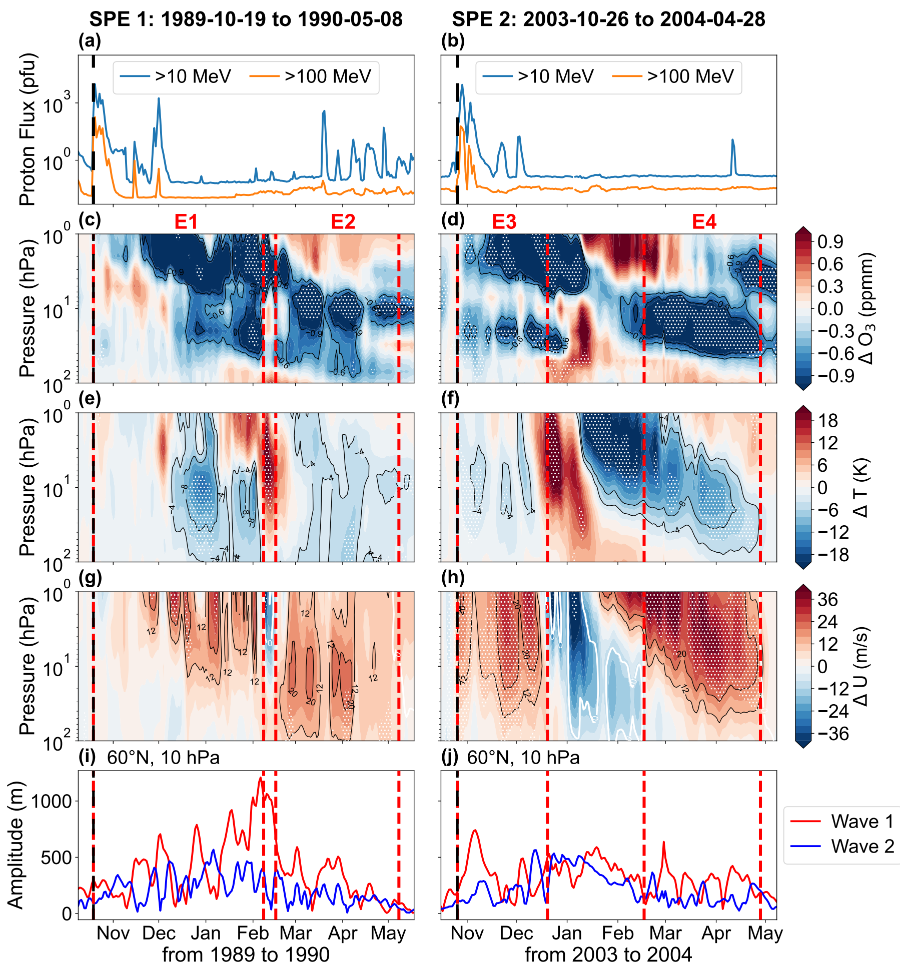

Figure 1. Time evolution of solar proton fluxes for (a) SPE1 and (b) SPE2, and the corresponding polar-cap (60°–90°N) anomalies of ozone (c, d), temperature (e, f), zonal-mean zonal wind (g, h), and PW amplitude (i, j) from the SPE onset to the subsequent springtime vortex breakdown for SPE1 and SPE2. Contours in panels (c–h) indicate the corresponding anomaly fields. The thick white contour in panels (g, h) denotes the 0 m s^{-1} isoline of the cosine-weighted polar-cap (60°–90°N) mean zonal wind (U_{6090}). White dots indicate anomalies exceeding the 90% confidence level based on the Monte Carlo test. The black dashed line marks the SPE onset, and the red dashed lines indicate the beginning and end of the identified APV response episodes.

https://doi.org/10.5194/egusphere-2026-4234
Preprint. Discussion started: 6 August 2026

Despite pronounced ozone depletion, the associated radiative cooling (Fig. 2a,b) remains weak during late autumn and winter. The absence of solar radiation largely suppresses shortwave radiative effects, while the longwave response is characterized by weak warming, resulting in only limited net radiative cooling (Fig. A1). As solar radiation returns in spring, ozone depletion exerts a stronger radiative influence and enhances the radiative cooling. Nevertheless, the radiative cooling remains approximately one order of magnitude smaller than the corresponding dynamical cooling throughout the response episodes (Fig. 2a–d). Consequently, changes in ozone radiative heating alone cannot account for the observed polar cooling or the accompanying vortex strengthening.

To quantify the relative importance of these two processes, we define the radiative–dynamical cooling dominance metric R (Fig. 2e,f). Throughout most response episodes and over most of the polar stratosphere, R remains close to -1, indicating that the cooling is overwhelmingly dominated by dynamical processes. Following the return of sunlight in spring, the radiative contribution becomes more important and R increases to approximately -0.9. However, dynamical cooling remains the dominant contributor throughout the response period.

This dominance of dynamical cooling is ultimately reflected in the net heating rate anomalies (Fig. 2g,h), which show good agreement with the temperature anomaly tendencies (Fig. 2i,j), with pattern correlation coefficients of 0.72 and 0.73 for the two events, respectively. Taken together, the dominance metric R, the net heating rate anomalies, and the temperature anomaly tendencies consistently indicate that the observed polar cooling is primarily maintained by dynamical processes rather than by direct radiative effects associated with ozone depletion. This motivates an examination of how PW activity modulates the residual circulation and thereby controls the dynamical heating.

3.3 PW forcing, residual circulation, and dynamical cooling

PWs influence the APV through both wave–mean flow interactions and their control of the residual circulation. In the TEM framework, by driving the residual circulation, wave drag regulates polar dynamical heating through adiabatic descent: enhanced wave drag strengthens polar downwelling and warming, whereas reduced wave drag favors cooling. We therefore examine changes in PW propagation, wave forcing, and residual circulation following the SPEs.

Fig. 3a–h shows latitude–pressure cross-sectional views of temperature and zonal wind for the four SPE episodes, while Fig. 4 presents the corresponding temperature and zonal wind anomalies at 10 hPa. All four episodes are characterized by pronounced cooling in the polar upper stratosphere (Fig. 3a–d), accompanied by strengthened high-latitude westerlies (Fig. 3e–h), indicating an intensified APV. The horizontal structures at 10 hPa are consistent with these zonal-mean responses, showing enhanced polar cooling surrounded by stronger circumpolar westerlies (Fig. 4). During E2, however, the cooling center is displaced away from the pole, resulting in a corresponding shift in the strongest wind anomalies.

Fig. 3i–l shows the wave diagnostics, and Fig. 3m–p shows the associated dynamical heating anomalies. Following SPE1 (Fig. 3i–j), the zero contour of refractive index forms a downward-sloping propagation boundary for PWs near 80°N, and it exhibits a downward-bending structure between approximately 65°N and 75°N in the upper stratosphere during E2. As EP-flux vectors approach the polar stratopause, they are progressively redirected downward, yielding a pronounced downward component over much of the 60°–80°N upper stratosphere (arrows in Fig. 3i–j). Positive wave forcing anomalies dominate

https://doi.org/10.5194/egusphere-2026-4234
Preprint. Discussion started: 6 August 2026

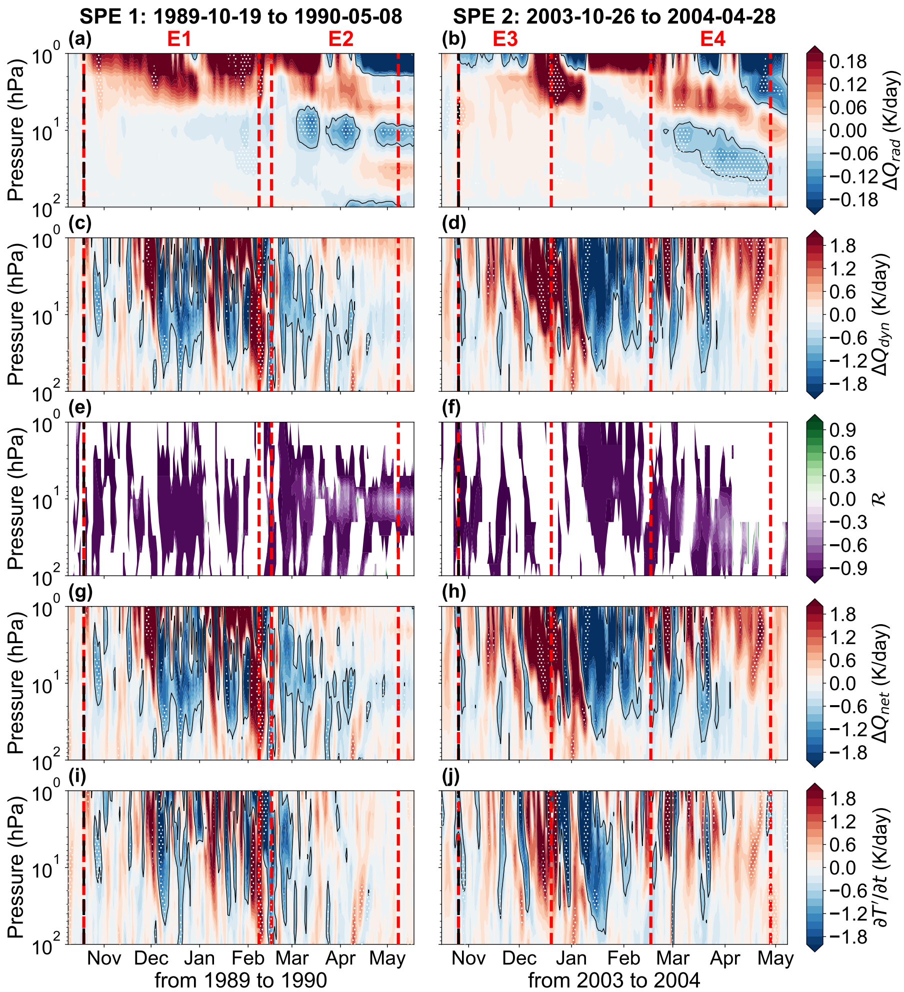

Figure 2. Time evolution of polar-cap (60°–90°N) anomalies of net radiative heating rates ($Q_{\rm rad}$; a, b), dynamical heating rates ($Q_{\rm dyn}$; c, d), the radiative–dynamical cooling dominance metric R (e, f), net heating rates (g, h), and temperature anomaly tendencies (i, j) from the SPE onset to the subsequent springtime vortex breakdown for SPE1 and SPE2. Values of R approaching -1 indicate cooling dominated by dynamical processes, whereas values approaching $+1$ indicate cooling dominated by radiative processes. Black contours denote anomalies of 0.06 K day^{-1} in panels (a, b) and 0.6 K day^{-1} in panels (c–d and g–j). White dots indicate anomalies exceeding the 90% confidence level based on the Monte Carlo test. The black dashed line marks the SPE onset, and the red dashed lines indicate the beginning and end of the identified APV response episodes.

https://doi.org/10.5194/egusphere-2026-4234
Preprint. Discussion started: 6 August 2026

the upper stratosphere poleward of approximately 50°N, indicating reduced wave drag. Correspondingly, weakened polar downwelling is accompanied by negative dynamical heating anomalies (Fig. 3m–n), indicating enhanced dynamical cooling and strengthened westerly anomalies (Fig. 3e–f).

Following SPE2 (Fig. 3k–l), the wave anomalies exhibit a more complex structure, likely reflecting the influence of the major SSW and the enhanced PW-2 activity (Fig. 1j). Similar to E1, the zero contour of refractive index forms a downward-sloping propagation boundary, beyond which the wave propagation is inhibited. In E3, the EP flux vectors propagate upward and poleward between approximately 50°N and 75°N before turning downward near the refractive index boundary at higher latitudes. In E4, the downward component becomes more pronounced, with EP flux vectors exhibiting a steeper descent angle compared to E3.

The wave forcing anomalies exhibit a vertically tilted dipole structure (Fig. 3k–l), characterized by negative anomalies over the polar cap and positive anomalies at lower latitudes. A similar tilted dipole structure is evident in the residual circulation and dynamical heating anomalies (Fig. 3o–p), with enhanced downwelling and dynamical heating on the poleward side and weakened downwelling associated with dynamical cooling equatorward. Despite this spatial complexity, the net effect over the polar cap is characterized by reduced dynamical heating in the middle and lower stratosphere, consistent with the dominant cooling anomalies identified in Fig. 2.

Together, these features suggest that the altered wave propagation weakens the wave-driven residual circulation over the polar cap, thereby suppressing dynamical heating and maintaining the cooling anomalies associated with the strengthened APV.

4 Discussion

Recently, Nesse et al. (2026) proposed that EPP-induced ozone depletion may influence stratospheric dynamics through thermal wind adjustment and subsequent wave–mean flow interactions. Key features of this mechanism, including polar ozone depletion (Szeląg et al., 2022; Wang et al., 2024), middle and lower stratospheric cooling (Seppälä et al., 2013; Arsenovic et al., 2016; Salminen et al., 2019, 2024; Asikainen et al., 2020), polar vortex strengthening (Seppälä et al., 2013; Arsenovic et al., 2016; Salminen et al., 2019, 2020a; Asikainen et al., 2020), and a reduction of Eliassen-Palm flux convergence (Seppälä et al., 2013; Salminen et al., 2024), have been reported in both modelling and observational studies (Nesse et al., 2026). Our analysis of two extreme SPEs on record provides reanalysis evidence for the spatiotemporal evolution of the atmospheric response from the SPE onset to the subsequent springtime vortex breakdown, together with quantitative diagnostics that support the proposed ozone–dynamics feedback under extreme forcing conditions.

Fig. 5 summarizes the dominant processes inferred from the two events. Extreme SPEs inject large fluxes of energetic protons into the polar middle atmosphere, producing substantial amounts of HO_x and NO_y through ionization. During the following months, the downward branch of the residual circulation transports EPP-produced NO_y from the mesosphere into the stratosphere, wherein the ozone destruction continues. Meanwhile, the strong APV suppresses mixing with ozone-rich mid-latitude air. As a result, substantial ozone depletion can persist from SPE onset to spring, qualitatively consistent with the

https://doi.org/10.5194/egusphere-2026-4234
Preprint. Discussion started: 6 August 2026

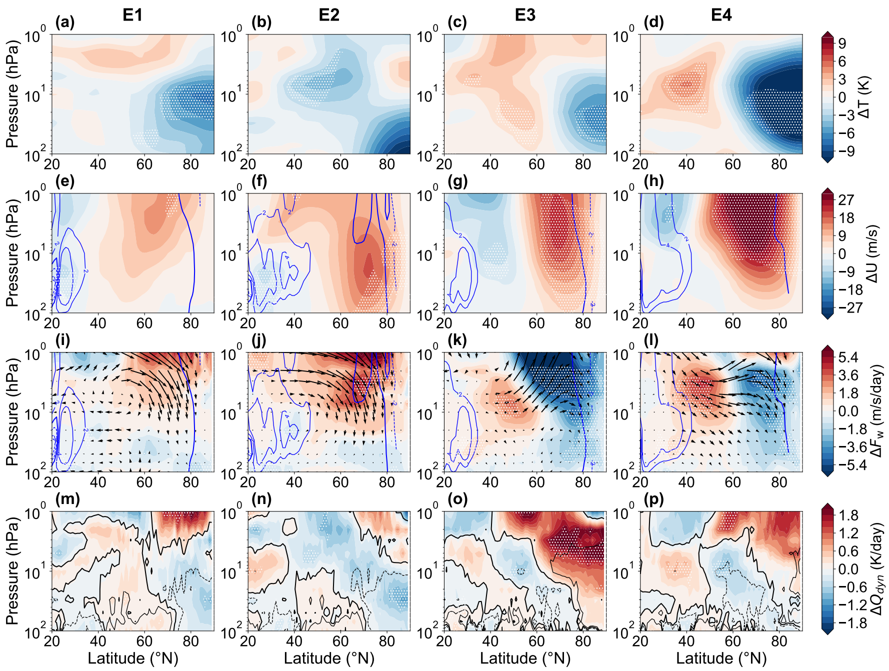

Figure 3. Pressure–latitude distributions of temperature anomalies (a–d), zonal wind anomalies (e–h), wave forcing anomalies (i–l), and dynamical heating anomalies (m–p) during the four APV response episodes. All anomaly fields are defined relative to the climatology and the 5-day pre-event baseline. Blue contours in panels (e–l) denote the refractive index (n^2), with thick blue contours indicating $n^2 = 0$. Arrows in panels (i–l) indicate EP flux vectors scaled by $\exp(z/H)$, approximately equivalent to dividing by density (Mechoso et al., 1985; G.J., 2020). The vertical component is further multiplied by 150 to improve visibility. Black contours in panels (m–p) denote residual circulation vertical velocity anomalies (w^*) scaled by 10^4; solid (positive) and dotted (negative) contours, respectively, and thick contours indicate zero values. White dots indicate anomalies exceeding the 90% confidence level based on the Monte Carlo test.

temporal evolution simulated by Whole Atmosphere Community Climate Model with D-region ion chemistry (WACCM-D) (Fig. B1). However, the magnitude of ozone loss is underestimated, which may be partly because the prescribed proton forcing does not include protons with energies above 300 MeV (Jia et al., 2020).

The ozone depletion reduces shortwave radiative heating, leading to cooling of the polar stratosphere (Szeląg et al., 2022) and an enhanced meridional temperature gradient. Through thermal wind balance, the strengthened temperature gradient intensifies the polar night jet and strengthens the APV (Zhao et al., 2025). This interpretation is consistent with the statistical relationship between SPE proton flux and concurrent APV strengthening reported by Li et al. (2025).

The strengthened vortex subsequently modifies PW propagation and wave–mean flow interactions (Zhao et al., 2025). Both events exhibit a tendency for PW activity to refract downward at high latitudes, although the associated EP-flux structures differ, likely because of their contrasting dynamical backgrounds. These changes are accompanied by a weakening of the residual circulation and enhanced dynamical cooling over the polar stratosphere. The resulting cooling further reinforces the

https://doi.org/10.5194/egusphere-2026-4234
Preprint. Discussion started: 6 August 2026

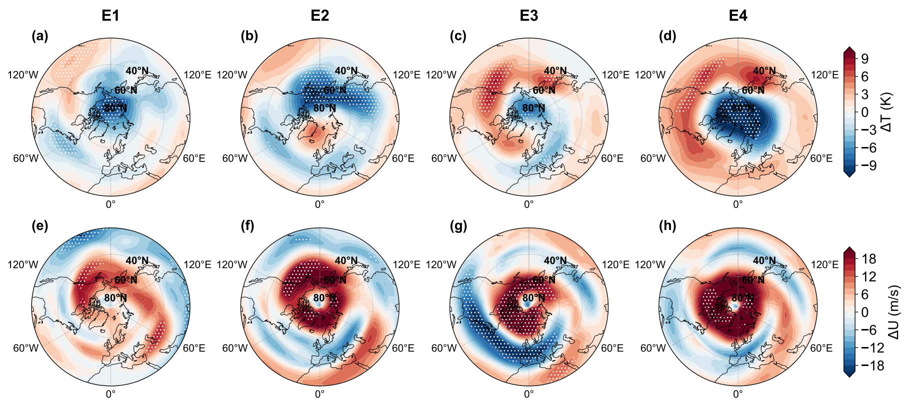

Figure 4. Spatial distributions of temperature anomalies (a–d) and zonal wind anomalies (e–h) at 10 hPa during the four APV response episodes (E1–E4). Anomalies are defined relative to the climatology and the 5-day pre-event baseline. White dots indicate anomalies exceeding the 90% confidence level based on the Monte Carlo test.

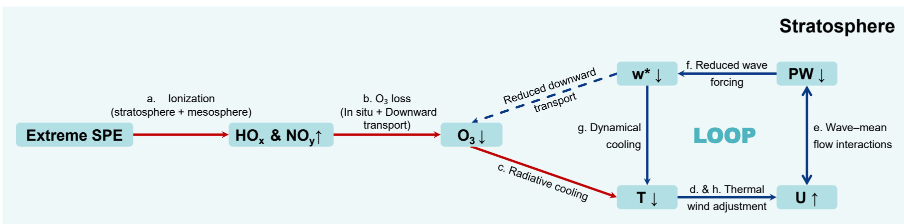

Figure 5. Schematic illustration of the positive ozone–dynamics feedback following extreme SPEs. Red arrows denote the chemical processes linking SPE-induced ionization to ozone depletion, whereas blue arrows denote the associated dynamical feedbacks. Blue dashed arrows indicate a potential subsequent modulation of ozone transport through changes in the residual circulation.

vortex, forming a positive dynamical feedback that may help maintain the SPE-induced anomaly from autumn into late winter and spring.

Previous studies have shown that springtime Arctic lower stratospheric temperature variability is controlled primarily by wave-driven dynamical processes (Newman et al., 2001). Consistent with this view, our thermodynamic budget diagnostics demonstrate that dynamical cooling associated with wave-driven residual circulation substantially exceeds the direct radiative cooling induced by ozone depletion. Together with the coherent evolution of ozone depletion, temperature anomalies, APV variability, and diagnosed wave–mean flow interactions, these results suggest that SPE-induced ozone loss may interact with stratospheric circulation and amplify APV anomalies through a positive ozone–dynamics feedback. However, the robustness and generality of this feedback require confirmation through larger-sample statistical analyses and dedicated model experiments.

Our results further suggest that the manifestation of the proposed ozone–dynamics feedback is strongly modulated by the background dynamical state of the winter stratosphere. The two extreme SPEs analyzed here represent two contrasting evolu-

https://doi.org/10.5194/egusphere-2026-4234
Preprint. Discussion started: 6 August 2026

tions of the APV under extreme particle forcing. Following SPE1, only a minor SSW occurred, and the APV remained largely stable throughout the winter, allowing the proposed feedback to develop continuously. In contrast, a major SSW occurred approximately two months after SPE2, substantially disrupting the APV and interrupting the persistence of the dynamical feedback. Under relatively stable dynamical conditions (E1–E3), the broadly coherent timing of ozone depletion and dynamical cooling, together with their distinct vertical structures, suggests an important dynamical contribution beyond the direct radiative effect of ozone depletion, consistent with the proposed ozone–dynamics feedback (Friedel et al., 2022). After the onset of the major SSW (E4), however, the SPE signal becomes increasingly difficult to distinguish from strong internal dynamical variability. Similar behaviour was observed during the winters of 2000 and 2001, when frequent SSW activity may have obscured any coherent SPE-induced dynamical response despite substantial proton fluxes reaching the stratosphere.

In this context, the dipole pattern in the PW anomalies resembles the structure identified by Salminen et al. (2022), who showed that EPP effects are most systematic when wave propagation is enhanced at mid-latitudes and reduced over the polar region. This suggests that the background wave configuration plays a key role in modulating the stratospheric response to energetic particle forcing. During SSWs, enhanced planetary wave activity reorganizes the residual circulation through wave–mean flow interactions and modifies the dynamical state of the winter stratosphere. As a result, the SPE-related signal is obscured by strong internal variability, limiting robust attribution of stratospheric changes to particle forcing. Whether EPP can influence the occurrence of SSWs remains uncertain (Salminen et al., 2020b; Edvartsen et al., 2023; Vokhmyanin et al., 2023; Nesse et al., 2026); addressing this question is beyond the scope of the present study.

The persistence of ozone, temperature, and circulation anomalies from late autumn into late winter and spring suggests that extreme SPEs may provide a source of subseasonal-to-seasonal predictability for the polar stratosphere. However, several limitations should be acknowledged. First, the present analysis is based on only two extreme events. Given the rarity of SPEs that are sufficiently intense to generate pronounced stratospheric responses, the availability of comparable events for such process-based analyses is inherently limited. Second, this study relies on ERA5 reanalysis and lacks direct observational constraints on key chemical species (e.g., NO_y), which limits a more comprehensive assessment of the chemical response. Third, because both events occurred under a similar QBO easterly phase, the QBO modulation of the SPE response could not be systematically assessed. Finally, the SPE-related signal cannot be fully separated from other EPP sources, such as EEP. Future studies combining long-term observations, chemistry climate model simulations, and larger event samples will be necessary to better quantify the dynamical influence of extreme SPEs on the winter polar atmosphere.

Despite these limitations, this study provides a detailed quantitative characterization of the temporal evolution of the stratospheric response to extreme SPEs, from initial ozone depletion in autumn to delayed vortex breakdown in spring. The consistency between the two events, despite their differing dynamical backgrounds, supports the existence of an ozone–dynamics feedback operating under extreme solar proton forcing.

https://doi.org/10.5194/egusphere-2026-4234
Preprint. Discussion started: 6 August 2026

5 Conclusions

Using GOES proton flux observations and ERA5 reanalysis data, we investigated the stratospheric response to two extreme SPEs that occurred in October 1989 and October 2003. Both events were followed by persistent ozone depletion, cooling of the polar stratosphere, and strengthening of the APV, with the temporal evolution of these anomalies remaining closely coupled from autumn into late winter and spring. In both cases, the vortex evolved from a relatively weak background state to a strongly enhanced state within the climatological distribution and remained anomalously strong for about six months. Thermodynamic budget diagnostics indicate that the temperature anomalies were dominated by dynamical cooling rather than direct radiative cooling associated with SPE-induced ozone loss. Although the two events occurred under markedly different winter dynamical conditions and exhibited distinct EP flux anomaly structures, both shared two common features: a tendency for PW activity to refract downward and net dynamical cooling over the polar stratosphere.

These results suggest that extreme SPEs can influence the winter polar stratosphere through a coupled ozone–dynamics pathway. Persistent ozone depletion reduces the shortwave heating and cools the polar stratosphere, strengthening the meridional temperature gradient and the APV through thermal wind adjustment. The strengthened APV may further alter PW propagation by wave–mean flow interactions, favoring dynamical cooling over the polar stratosphere. This cooling, in turn, reinforces the vortex, thereby closing a positive ozone-dynamics feedback loop.

By examining the temporal evolution of atmospheric anomalies following two extreme SPEs, this study provides process-based evidence supporting the ozone–dynamics feedback pathway. The persistence of ozone, temperature, and circulation anomalies suggests that extreme SPEs might influence the winter polar stratosphere on subseasonal to seasonal timescales. The contrasting responses observed under minor- and major-SSW conditions further indicate that the impact of SPEs depends strongly on the background dynamical state. These findings highlight the importance of accounting for EPP forcing in subseasonal-to-seasonal prediction systems that aim at improving the representation and predictability of winter polar stratospheric variability. More broadly, extreme SPEs provide a natural experiment for investigating the coupling between atmospheric composition and dynamics under strong external forcing. Future work combining observations and model simulations will help clarify the role of EPP in chemical–dynamical coupling and its contribution to variability and predictability in the winter polar stratosphere. Despite the limited sample size, the consistency of the response across two extreme events with contrasting dynamical backgrounds lends confidence to the existence of a robust ozone–dynamics feedback under strong solar proton forcing.

Appendix A: Shortwave and longwave radiative heating rates calculated using RRTMG

Figure A1 decomposes the net radiative heating anomalies (Figure 2) into shortwave (Q_{sw}) and longwave (Q_{lw}) components. During the polar night (E1 and E3), ozone depletion produces little shortwave radiative cooling because of the absence of solar radiation, whereas the longwave component exhibits weak warming that partly offsets the cooling in the middle and lower stratosphere. As sunlight returns in spring (E2 and E4), shortwave cooling becomes increasingly pronounced and dominates

https://doi.org/10.5194/egusphere-2026-4234
Preprint. Discussion started: 6 August 2026

the net radiative response to ozone depletion, while longwave anomalies remain comparatively small. These results provide a
340 more detailed view of the radiative evolution associated with SPE-induced ozone depletion.

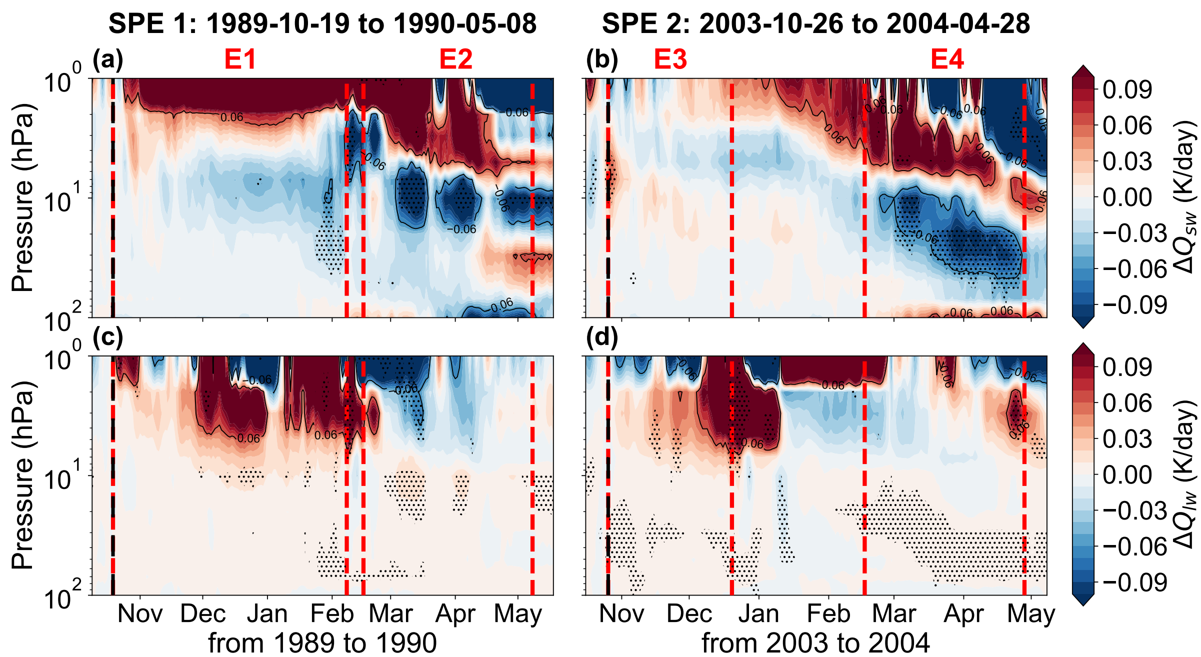

Figure A1. Time evolution of polar-cap (60°–90°N) anomalies of ozone-induced shortwave (Q_{sw}; a, b) and longwave (Q_{lw}; c, d) radiative heating rates from the SPE onset to the subsequent springtime vortex breakdown for SPE1 and SPE2. Contours show the corresponding anomaly fields. Black dots indicate anomalies exceeding the 90% confidence level based on the Monte Carlo test. The black dashed line marks the SPE onset, and the red dashed lines indicate the beginning and end of the identified APV response episodes.

Appendix B: WACCM-D simulations of SPE-induced chemical perturbations

WACCM-D has been widely used to investigate the impacts of EPP on the polar middle atmosphere (Verronen et al., 2016). We have conducted WACCM simulations in order to provide supporting evidence for the chemical perturbations associated with the two SPEs. The model was run in the specified dynamics (SD) configuration using ERA5 reanalysis data. It has a
345 horizontal resolution of $1.25°$ longitude by $0.94°$ latitude and 88 vertical levels extending from the surface to 6×10^{-6} hPa (approximately 140 km).

Only solar proton forcing was included in the experiments. Differences between simulations with and without SPE forcing were calculated to isolate the SPE-induced changes in NO_y and O_3. The model results are presented as supporting evidence for the chemical pathways discussed in this study. The WACCM-D simulation tends to underestimate the magnitude of ozone
350 depletion compared to observations (Jia et al., 2020).

https://doi.org/10.5194/egusphere-2026-4234
Preprint. Discussion started: 6 August 2026

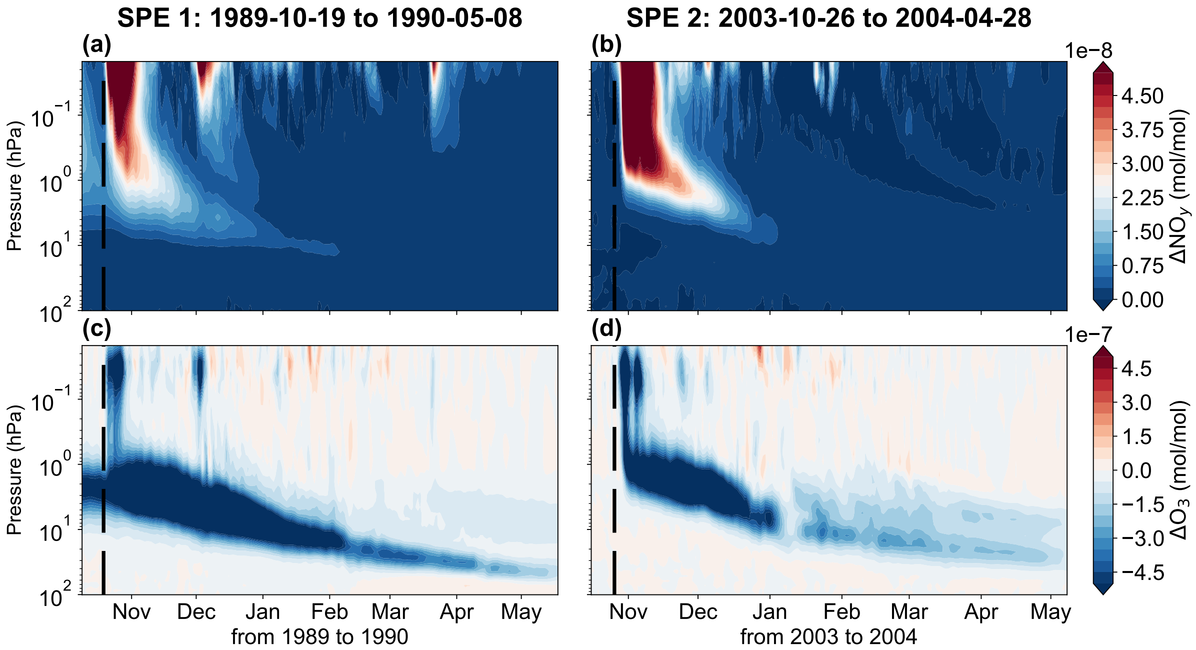

Figure B1. Time evolution of WACCM-D simulated polar-cap (60°–90°N) anomalies in NO_y (a,b) and O_3 (c,d) from the SPE onset to the subsequent springtime vortex breakdown for SPE1 and SPE2. Anomalies are calculated as the differences between simulations with and without SPE forcing and are shown from the SPE onset to the subsequent springtime vortex breakdown. The black dashed line marks the SPE onset.

Code and data availability. ERA5 reanalysis data are publicly available from the Copernicus Climate Data Store (https://cds.climate.copernicus.eu/datasets/reanalysis-era5-pressure-levels?tab=download or https://doi.org/10.24381/cds.bd0915c6). Solar proton flux observations from GOES satellites are publicly available from NOAA (https://www.ngdc.noaa.gov/stp/satellite/goes/dataaccess.html). Offline radiative transfer calculations were performed using the publicly available climlab Python package interfaced with RRTMG (https://climlab.readthedocs.io/en/latest/api/climlab.radiation.RRTMG.html).

Author contributions. Y. Li conceived the study, performed the analysis, and prepared the original manuscript draft. H. Li supervised the project, secured funding, contributed to the interpretation of the results, and revised the manuscript. Y. Wang and Y. Liu contributed to data preparation and provided methodological support for the analysis. Y. Pan and W. Xu performed the WACCM-D model simulations. C. Wang provided supervision and contributed to the discussion of the study. All authors contributed to the discussion of the results and approved the final manuscript.

Competing interests. The authors declare that they have no conflict of interest.

https://doi.org/10.5194/egusphere-2026-4234
Preprint. Discussion started: 6 August 2026

Acknowledgements. This work was supported by the National Key R&D Program of China (2025YFE0202500), NNSFC grants (42374198, 42188101), project of Civil Aerospace "14th Five Year Plan" Preliminary Research in Space Science (D010301, D010202). H. Li was also supported by the China-Brazil Joint Laboratory for Space Weather grant (119GJHZ2024027MI) and in part by the Specialized Research
365 Fund for State Key Laboratories of China. We thank C3S and ECMWF for providing the ERA5 data. This work was carried out as part of the International Space Science Institute (ISSI) project "Dynamical Signatures of Energetic Particle Precipitation in Atmospheric Re-analyses". We appreciate the fruitful discussions with the group members in this project.

References

Andrews, D. G., Holton, J. R., and Leovy, C. B.: Middle Atmosphere Dynamics, no. v. 40 in International Geophysics Series, Academic Press, Orlando, 1987.

Arsenovic, P., Rozanov, E., Stenke, A., Funke, B., Wissing, J. M., Mursula, K., Tummon, F., and Peter, T.: The Influence of Middle Range Energy Electrons on Atmospheric Chemistry and Regional Climate, Journal of Atmospheric and Solar-Terrestrial Physics, 149, 180–190, https://doi.org/10.1016/j.jastp.2016.04.008, 2016.

Asikainen, T., Salminen, A., Maliniemi, V., and Mursula, K.: Influence of Enhanced Planetary Wave Activity on the Polar Vortex Enhancement Related to Energetic Electron Precipitation, Journal of Geophysical Research: Atmospheres, 125, https://doi.org/10.1029/2019JD032137, 2020.

Baldwin, M. P., Ayarzagüena, B., Birner, T., Butchart, N., Butler, A. H., Charlton-Perez, A. J., Domeisen, D. I. V., Garfinkel, C. I., Garny, H., Gerber, E. P., Hegglin, M. I., Langematz, U., and Pedatella, N. M.: Sudden Stratospheric Warmings, Reviews of Geophysics, 59, e2020RG000 708, https://doi.org/10.1029/2020RG000708, 2021.

Butchart, N.: The Stratosphere: A Review of the Dynamics and Variability, Weather and Climate Dynamics, 3, 1237–1272, https://doi.org/10.5194/wcd-3-1237-2022, 2022.

Butler, A. H., Seidel, D. J., Hardiman, S. C., Butchart, N., Birner, T., and Match, A.: Defining Sudden Stratospheric Warmings, Bulletin of the American Meteorological Society, 96, 1913–1928, https://doi.org/10.1175/BAMS-D-13-00173.1, 2015.

Denton, M. H., Kivi, R., Ulich, T., Clilverd, M. A., Rodger, C. J., and Von Der Gathen, P.: Northern Hemisphere Stratospheric Ozone Depletion Caused by Solar Proton Events: The Role of the Polar Vortex, Geophysical Research Letters, 45, 2115–2124, https://doi.org/10.1002/2017GL075966, 2018.

Edvartsen, J. Ø., Maliniemi, V., and Nesse, H.: Effects of Energetic Particle Precipitation on Stratospheric Temperature during Disturbed Stratospheric Polar Vortex Conditions, Journal of Geophysical Research: Atmospheres, 128, e2022JD038 010, https://doi.org/10.1029/2022JD038010, 2023.

Friedel, M., Chiodo, G., Stenke, A., Domeisen, D. I. V., Fueglistaler, S., Anet, J. G., and Peter, T.: Springtime Arctic Ozone Depletion Forces Northern Hemisphere Climate Anomalies, Nature Geoscience, 15, 541–547, https://doi.org/10.1038/s41561-022-00974-7, 2022.

Funke, B., Baumgaertner, A., Calisto, M., Egorova, T., Jackman, C. H., Kieser, J., Krivolutsky, A., López-Puertas, M., Marsh, D. R., Reddmann, T., Rozanov, E., Salmi, S.-M., Sinnhuber, M., Stiller, G. P., Verronen, P. T., Versick, S., von Clarmann, T., Vyushkova, T. Y., Wieters, N., and Wissing, J. M.: Composition Changes after the "Halloween" Solar Proton Event: The High Energy Particle Precipitation in the Atmosphere (HEPPA) Model versus MIPAS Data Intercomparison Study, Atmospheric Chemistry and Physics, 11, 9089–9139, https://doi.org/10.5194/acp-11-9089-2011, 2011.

G.J., B.: Low Latitude Dynamical Response to Vortex Split Sudden Stratospheric Warming: An Eliassen Palm Flux Perspective, Dynamics of Atmospheres and Oceans, 91, 101 146, https://doi.org/10.1016/j.dynatmoce.2020.101146, 2020.

Hannachi, A., Lechner, M., Finke, K., and Mukhin, D.: Stratospheric Polar Vortex, Wave Absorption/Reflection and Effect on Surface Climate, Climate Dynamics, 63, 126, https://doi.org/10.1007/s00382-025-07610-1, 2025.

Hauchecorne, A., Claud, C., Keckhut, P., and Mariaccia, A.: Stratospheric Final Warmings Fall into Two Categories with Different Evolution over the Course of the Year, Communications Earth & Environment, 3, 4, https://doi.org/10.1038/s43247-021-00335-z, 2022.

Hersbach, H., Bell, B., Berrisford, P., Hirahara, S., Horányi, A., Muñoz-Sabater, J., Nicolas, J., Peubey, C., Radu, R., Schepers, D., Simmons, A., Soci, C., Abdalla, S., Abellan, X., Balsamo, G., Bechtold, P., Biavati, G., Bidlot, J., Bonavita, M., Chiara, G., Dahlgren, P., Dee, D., Dia-

https://doi.org/10.5194/egusphere-2026-4234
Preprint. Discussion started: 6 August 2026

mantakis, M., Dragani, R., Flemming, J., Forbes, R., Fuentes, M., Geer, A., Haimberger, L., Healy, S., Hogan, R. J., Hólm, E., Janisková, M., Keeley, S., Laloyaux, P., Lopez, P., Lupu, C., Radnoti, G., Rosnay, P., Rozum, I., Vamborg, F., Villaume, S., and Thépaut, J.-N.: The ERA5 Global Reanalysis, Quarterly Journal of the Royal Meteorological Society, 146, 1999–2049, https://doi.org/10.1002/qj.3803, 2020.

Hersbach, H., Bell, B., Berrisford, P., Biavati, G., Horányi, A., Muñoz Sabater, J., Nicolas, J., Peubey, C., Radu, R., Rozum, I., Schepers, D., Simmons, A., Soci, C., Dee, D., and Thépaut, J.-N.: ERA5 hourly data on pressure levels from 1940 to present, https://doi.org/10.24381/cds.bd0915c6, accessed on 30 June 2026, 2023.

Hong, H.-J., Reichler, T., and Hsu, H.-H.: Arctic Ozone Amplifies Stratospheric Circulation Extremes, Journal of Climate, 38, 5491–5503, https://doi.org/10.1175/JCLI-D-24-0446.1, 2025.

Iacono, M. J., Delamere, J. S., Mlawer, E. J., Shephard, M. W., Clough, S. A., and Collins, W. D.: Radiative Forcing by Long-Lived Greenhouse Gases: Calculations with the AER Radiative Transfer Models, Journal of Geophysical Research: Atmospheres, 113, https://doi.org/10.1029/2008JD009944, 2008.

Jackman, C. H., Marsh, D. R., Vitt, F. M., Garcia, R. R., Fleming, E. L., Labow, G. J., Randall, C. E., López-Puertas, M., Funke, B., Von Clarmann, T., and Stiller, G. P.: Short- and Medium-Term Atmospheric Constituent Effects of Very Large Solar Proton Events, Atmospheric Chemistry and Physics, 8, 765–785, https://doi.org/10.5194/acp-8-765-2008, 2008.

Jia, J., Kero, A., Kalakoski, N., Szeląg, M. E., and Verronen, P. T.: Is There a Direct Solar Proton Impact on Lower-Stratospheric Ozone?, Atmospheric Chemistry and Physics, 20, 14 969–14 982, https://doi.org/10.5194/acp-20-14969-2020, 2020.

Jia, J., Murberg, L. E., Løvset, T., Orsolini, Y. J., Espy, P. J., Zeller, L. C. G., Salinas, C. C. J. H., Lee, J. N., Wu, D., and Zhang, J.: Energetic Particle Precipitation Influences Global Secondary Ozone Distribution, Communications Earth & Environment, 5, 1–11, https://doi.org/10.1038/s43247-024-01419-2, 2024.

Klocke, D., Quaas, J., and Stevens, B.: Assessment of Different Metrics for Physical Climate Feedbacks, Climate Dynamics, 41, 1173–1185, https://doi.org/10.1007/s00382-013-1757-1, 2013.

Li, H., Li, Y., Wang, Y., Sun, J., and Wang, C.: Impact of Solar Proton Events on the Stratospheric Polar Vortex in the Northern Hemisphere: A Quantitative Analysis, Journal of Geophysical Research: Space Physics, 130, e2024JA033 068, https://doi.org/10.1029/2024JA033068, 2025.

Li, Q., Graf, H.-F., and Giorgetta, M. A.: Stationary Planetary Wave Propagation in Northern Hemisphere Winter – Climatological Analysis of the Refractive Index, Atmospheric Chemistry and Physics, 7, 183–200, https://doi.org/10.5194/acp-7-183-2007, 2007.

Liu, J., Zhang, D., Sun, S., Hao, Y., and Xiao, Z.: Latitudinal and Interhemispheric Differences of the Ionospheric Semi-Diurnal Lunitidal Perturbations during the 2009 Arctic Sudden Stratospheric Warming Event in the Eastern Asia–Australia Sector, Earth, Planets and Space, 74, 22, https://doi.org/10.1186/s40623-022-01581-x, 2022.

Matsuno, T.: Vertical Propagation of Stationary Planetary Waves in the Winter Northern Hemisphere, Journal of the Atmospheric Sciences, 27, 871–883, https://doi.org/10.1175/1520-0469(1970)027<0871:VPOSPW>2.0.CO;2, 1970.

Mechoso, C. R., Hartmann, D. L., and Farrara, J. D.: Climatology and Interannual Variability of Wave, Mean-Flow Interaction in the Southern Hemisphere, Journal of the Atmospheric Sciences, 42, 2189–2206, https://doi.org/10.1175/1520-0469(1985)042<2189:CAIVOW>2.0.CO;2, 1985.

Mlawer, E. J., Taubman, S. J., Brown, P. D., Iacono, M. J., and Clough, S. A.: Radiative Transfer for Inhomogeneous Atmospheres: RRTM, a Validated Correlated-k Model for the Longwave, Journal of Geophysical Research: Atmospheres, 102, 16 663–16 682, https://doi.org/10.1029/97JD00237, 1997.

Nesse, H., Asikainen, T., Decotte, M., Funke, B., Harvey, V. L., Jia, J., Liu, H., Liu, H., Maliniemi, V., Partamies, N., Salice, J. A., Salminen, A., Seppälä, A., Stephan, C. C., and Vokhmyanin, M.: Why Is Energetic Particle Precipitation Important for Climate Research and Seasonal Forecasting?, Surveys in Geophysics, https://doi.org/10.1007/s10712-026-09946-7, 2026.

Newman, P. A., Nash, E. R., and Rosenfield, J. E.: What Controls the Temperature of the Arctic Stratosphere during the Spring?, Journal of Geophysical Research: Atmospheres, 106, 19 999–20 010, https://doi.org/10.1029/2000JD000061, 2001.

Oehrlein, J., Chiodo, G., and Polvani, L. M.: The Effect of Interactive Ozone Chemistry on Weak and Strong Stratospheric Polar Vortex Events, Atmospheric Chemistry and Physics, 20, 10 531–10 544, https://doi.org/10.5194/acp-20-10531-2020, 2020.

Rieger, V. S., Dietmüller, S., and Ponater, M.: Can Feedback Analysis Be Used to Uncover the Physical Origin of Climate Sensitivity and Efficacy Differences?, Climate Dynamics, 49, 2831–2844, https://doi.org/10.1007/s00382-016-3476-x, 2017.

Rozanov, E., Calisto, M., Egorova, T., Peter, T., and Schmutz, W.: Influence of the Precipitating Energetic Particles on Atmospheric Chemistry and Climate, Surveys in Geophysics, 33, 483–501, https://doi.org/10.1007/s10712-012-9192-0, 2012.

Salminen, A., Asikainen, T., Maliniemi, V., and Mursula, K.: Effect of Energetic Electron Precipitation on the Northern Polar Vortex: Explaining the QBO Modulation via Control of Meridional Circulation, Journal of Geophysical Research: Atmospheres, p. 2018JD029296, https://doi.org/10.1029/2018JD029296, 2019.

Salminen, A., Asikainen, T., Maliniemi, V., and Mursula, K.: Comparing the Effects of Solar-Related and Terrestrial Drivers on the Northern Polar Vortex, Journal of Space Weather and Space Climate, 10, 56, https://doi.org/10.1051/swsc/2020058, 2020a.

Salminen, A., Asikainen, T., Maliniemi, V., and Mursula, K.: Dependence of Sudden Stratospheric Warmings on Internal and External Drivers, Geophysical Research Letters, 47, e2019GL086 444, https://doi.org/10.1029/2019GL086444, 2020b.

Salminen, A., Asikainen, T., and Mursula, K.: Planetary Waves Controlling the Effect of Energetic Electron Precipitation on the Northern Polar Vortex, Geophysical Research Letters, 49, https://doi.org/10.1029/2021GL097076, 2022.

Salminen, A., Asikainen, T., and Mursula, K.: Satellite Observations of the Influence of Energetic Electron Precipitation on the Mesosphere and Stratosphere in the Northern Hemisphere, Journal of Geophysical Research: Atmospheres, 129, e2023JD039 581, https://doi.org/10.1029/2023JD039581, 2024.

Schoeberl, M. and Newman, P.: MIDDLE ATMOSPHERE | Polar Vortex, in: Encyclopedia of Atmospheric Sciences, pp. 12–17, Elsevier, https://doi.org/10.1016/B978-0-12-382225-3.00228-0, 2015.

Seppälä, A., Lu, H., Clilverd, M. A., and Rodger, C. J.: Geomagnetic Activity Signatures in Wintertime Stratosphere Wind, Temperature, and Wave Response: STRATOSPHERE AND GEOMAGNETIC ACTIVITY, Journal of Geophysical Research: Atmospheres, 118, 2169–2183, https://doi.org/10.1002/jgrd.50236, 2013.

Seppälä, A., Matthes, K., Randall, C. E., and Mironova, I. A.: What Is the Solar Influence on Climate? Overview of Activities during CAWSES-II, Progress in Earth and Planetary Science, 1, 24, https://doi.org/10.1186/s40645-014-0024-3, 2014.

Seppälä, A., Kalakoski, N., Verronen, P. T., Marsh, D. R., Karpechko, A. Y., and Szelag, M. E.: Polar Mesospheric Ozone Loss Initiates Downward Coupling of Solar Signal in the Northern Hemisphere, Nature Communications, 16, 748, https://doi.org/10.1038/s41467-025-55966-z, 2025.

Shi, Y., Evtushevsky, O., Shulga, V., Milinevsky, G., Klekociuk, A., Andrienko, Y., and Han, W.: Mid-Latitude Mesospheric Zonal Wave 1 and Wave 2 in Recent Boreal Winters, Remote Sensing, 13, 3749, https://doi.org/10.3390/rs13183749, 2021.

Silverman, V., Harnik, N., Matthes, K., Lubis, S. W., and Wahl, S.: Radiative Effects of Ozone Waves on the Northern Hemisphere Polar Vortex and Its Modulation by the QBO, Atmospheric Chemistry and Physics, 18, 6637–6659, https://doi.org/10.5194/acp-18-6637-2018, 2018.

https://doi.org/10.5194/egusphere-2026-4234
Preprint. Discussion started: 6 August 2026

Smith-Johnsen, C., Nesse Tyssøy, H., Hendrickx, K., Orsolini, Y., Kishore Kumar, G., Ødegaard, L.-K. G., Sandanger, M. I., Stordal, F., and Megner, L.: Direct and Indirect Electron Precipitation Effect on Nitric Oxide in the Polar Middle Atmosphere, Using a Full-range Energy Spectrum, Journal of Geophysical Research: Space Physics, 122, 8679–8693, https://doi.org/10.1002/2017JA024364, 2017.

Szeląg, M. E., Marsh, D. R., Verronen, P. T., Seppälä, A., and Kalakoski, N.: Ozone Impact from Solar Energetic Particles Cools the Polar Stratosphere, Nature Communications, 13, 6883, https://doi.org/10.1038/s41467-022-34666-y, 2022.

Tian, W., Huang, J., Zhang, J., Xie, F., Wang, W., and Peng, Y.: Role of Stratospheric Processes in Climate Change: Advances and Challenges, Advances in Atmospheric Sciences, 40, 1379–1400, https://doi.org/10.1007/s00376-023-2341-1, 2023.

Turunen, E., Verronen, P. T., Seppälä, A., Rodger, C. J., Clilverd, M. A., Tamminen, J., Enell, C.-F., and Ulich, T.: Impact of Different Energies of Precipitating Particles on NOx Generation in the Middle and Upper Atmosphere during Geomagnetic Storms, Journal of Atmospheric and Solar-Terrestrial Physics, 71, 1176–1189, https://doi.org/10.1016/j.jastp.2008.07.005, 2009.

Veretenenko, S. V.: Effects of Energetic Solar Proton Events of Solar Cycle 23 on Intensity of the Stratospheric Polar Vortex, Geomagnetism and Aeronomy, 61, 985–992, https://doi.org/10.1134/S0016793221070227, 2021.

Verronen, P. T., Andersson, M. E., Marsh, D. R., Kovács, T., and Plane, J. M. C.: WACCM-D—Whole Atmosphere Community Climate Model with D-region Ion Chemistry, Journal of Advances in Modeling Earth Systems, 8, 954–975, https://doi.org/10.1002/2015MS000592, 2016.

Vokhmyanin, M., Asikainen, T., Salminen, A., and Mursula, K.: Long-Term Prediction of Sudden Stratospheric Warmings With Geomagnetic and Solar Activity, Journal of Geophysical Research: Atmospheres, 128, e2022JD037 337, https://doi.org/10.1029/2022JD037337, 2023.

Wang, Y., Li, H., and Wang, C.: Impact Pattern of Energetic Particle Precipitation on Polar Mesospheric Ozone, Journal of Geophysical Research: Space Physics, 129, e2024JA032 877, https://doi.org/10.1029/2024JA032877, 2024.

Ward, W., Seppälä, A., Yiğit, E., Nakamura, T., Stolle, C., Laštovička, J., Woods, T. N., Tomikawa, Y., Lübken, F.-J., Solomon, S. C., Marsh, D. R., Funke, B., and Pallamraju, D.: Role of the Sun and the Middle Atmosphere/Thermosphere/Ionosphere in Climate (ROSMIC): A Retrospective and Prospective View, Progress in Earth and Planetary Science, 8, 47, https://doi.org/10.1186/s40645-021-00433-8, 2021.

Waugh, D. W., Sobel, A. H., and Polvani, L. M.: What Is the Polar Vortex and How Does It Influence Weather?, Bulletin of the American Meteorological Society, 98, 37–44, https://doi.org/10.1175/BAMS-D-15-00212.1, 2017.

Wetherald, R. T. and Manabe, S.: Cloud Feedback Processes in a General Circulation Model, Journal of the Atmospheric Sciences, 45, 1397–1416, https://doi.org/10.1175/1520-0469(1988)045<1397:CFPIAG>2.0.CO;2, 1988.

Zhao, S., Zhang, J., Xia, X., Wang, Z., and Zhang, C.: Effects of Ozone–Climate Interactions on the Long-Term Temperature Trend in the Arctic Stratosphere, Atmospheric Chemistry and Physics, 25, 11 557–11 573, https://doi.org/10.5194/acp-25-11557-2025, 2025.